Journal of Applied Fluid Mechanics, Vol. 12, No. 1, pp. 257-269, 2019.
Available online at www.jafmonline.net, ISSN 1735-3572, EISSN 1735-3645.
DOI: 10.29252/jafm.75.253.29020

Study on Effects of Prandtl Number on Cross Buoyancy Flow past a Square Cylinder using OpenFOAM

S. Tanweer, A. Dewan† and S. Sanghi

Department of Applied Mechanics, Indian Institute of Technology Delhi Hauz Khas, New Delhi - 110016, India

†*Corresponding Author Email*: *dewan_anupam@yahoo.com*

(Received March 18, 2018; accepted September 1, 2018)

ABSTRACT

The influence of Prandtl number on laminar, unsteady flow past a heated square cylinder placed in a free-stream has been studied computationally. The flow has been investigated for $0.02 < Pr < 100$ at $Re = 100$ and $Ri = 1$. Effects of Prandtl number in unsteady mixed convection flow have been reported for the first time in the present study. The finite-volume based open source code OpenFOAM was used for the numerical simulations. An efficient algorithm (PIMPLE) has been used for the pressure-velocity coupling. Streamlines, isotherms, vorticity production and force coefficients have been studied in detail. The role of buoyancy on the baroclinic production has been discussed. Variation of lift coefficient with *Pr* was found to be quite interesting. The mean lift coefficient was found to be negative at low values of *Pr* but surprisingly it became positive at very high values of *Pr*.

Keywords: Prandtl number; Mixed convection; OpenFOAM; Baroclinic production; Lift coefficient.

NOMENCLATURE

C_D	drag coefficient
C_L	lift coefficient
C_P	pressure coefficient
D	height of the square cylinder
f	frequency of vortex shedding
Nu	Nusselt number
Pr	Prandtl number
Re	Reynolds number
Ri	Richardson number
t	nondimensional time
T_h	temperature of the cylinder surfaces
T_∞	free stream temperature
St	Strouhal number
U_∞	free stream velocity
u	velocity in streamwise direction
v	velocity in transverse direction
θ	nondimensional temperature

1. INTRODUCTION

The mixed convection flow past a heated bluff body of square cross-section is a fundamental problem of engineering interest and is encountered in many practical applications, such as, flow in heat exchangers, chemical industries, electronic cooling, flow around buildings, etc. Flow around unheated square obstacles involves the interaction of free shear-layer, boundary-layer formed on the body's surfaces and the wake formed behind the body. If cylinder is heated, the superimposed buoyancy makes the flow quite complex. Buoyancy effect is measured by a non-dimensional parameter called Richardson number, which is the ratio of the buoyancy force to the inertial force. The flow field around a heated body depends mainly on Reynolds number (*Re*), Richardson number (*Ri*) and Prandtl number (*Pr*). Experimental and numerical studies have been reported to investigate the influence of these parameters on flow field.

Some researchers have reported the influence of *Re* on flow over a square cylinder (Franke *et al.* 1990; Norberg *et al.* 1995; Robichaux *et al.* 1999). If cylinder is placed in a free-stream, then flow is steady for $Re < 40$ and unsteady for $Re > 50$ (Sharma and Eswaran 2004a). At low values of *Re* separation does not occur at front and rear corners of the cylinder and hence top and bottom surfaces behave as a flat plate. Due to this behavior heat transfer is maximum at these surfaces near the front corners and it decreases towards the rear corners (Rahnama and Hadi-Moghaddam 2005). At a high value of *Re*, flow separates at the leading edge of the cylinder and

forms a central shear-layer, below which a high turbulence intensity reverse flow region is formed (Lyn and Rodi 1994). The separated shear-layers are reattached on the top and bottom surfaces of the cylinder when the width-to-height (R) ratio of the cylinder exceeds 0.67 (Nakaguchi *et al.* 1968) and influence the heat transfer from the cylinder (Igarashi 1987). The highest heat transfer rate was observed for R = 0.62 (Ranjan and Dewan 2016). In case of shear-flow past a square cylinder, for low values of *Re*, small values of shear could cause unsteadiness in the flow and vice versa. Further, the flow becomes asymmetric with an increase in shear rate (Cheng *et al.* 2007).

Influence of buoyancy on flow field around a square cylinder has been studied by many researchers. In case of a cross buoyancy flow, vortex shedding occurs for all values of *Ri* in unsteady flow regime (Bhattacharyya and Mahapatra 2005) while onset of vortex shedding occurs after a critical value of *Ri* in a steady flow regime (Chatterjee and Mondal 2011). In case of aiding buoyancy, suppression of vortex shedding occurs after a critical value of *Ri* (Sharma and Eswaran 2004b; Chatterjee and Mondal 2011). The value of *Re* required for the onset of flow separation increases with value of *Ri* (Sharma *et al.* 2012). It was observed that the vortex formation length increased with *Ri* which caused a suppression of vortex shedding (Singh *et al.* 2007). In other words, buoyancy plays dual role. It stabilizes the flow in case of aiding buoyancy. On the other hand, it destabilizes the flow in case of a cross buoyancy (Chatterjee 2014). It was observed that the component of the baroclinic vorticity rate along the interface of counter-rotating vortices was responsible for the suppression of vortex shedding (Hassan and Ali 2013). It was showed that cylinder orientation with free-stream caused a destabilization of its wake (Kakade *et al.* 2010).

Another important parameter that can influence the flow field is Prandtl number (*Pr*). It is expressed as the ratio of the momentum diffusivity to the thermal diffusivity of the fluid. It varies in wide range, from approximately 0.001 for liquid metals to 10^{25} for earth's mantle. Fluids with different values of *Pr* are widely used in chemical industries and nuclear reactors. However only few studies have been reported to investigate the influence of *Pr* on flow past a square cylinder. Dhiman *et al.* (2008) examined the influence of *Pr* for the confined cross buoyancy flow past a square cylinder placed in a channel in a steady flow regime for 0.7 < *Pr* < 100. They reported behavior of streamlines, isotherms and drag and lift coefficients for various values of *Pr*. Sahu *et al.* (2009) studied the role of *Pr* on unsteady forced convection past a square cylinder. They showed that the Nusselt number over the cylinder surface increased with *Pr*. Chatterjee and Biswas (2011) investigated flow past a tandem square cylinder for a steady, forced convection for *Pr* in the range of 0.7 to 1000. They reported that at low values of *Pr* the isotherms were wider and at high values of *Pr* the isotherms became narrower due to a reduction in the thermal diffusion. Chatterjee and Amiroudine (2010) studied a cross buoyancy flow past a tandem square cylinder for 0.7 < *Pr* < 100 in a steady flow regime. They observed that buoyancy induced asymmetry in the flow field decreased with an increase in the value of *Pr*. Further they observed that variation of the lift coefficient with *Ri* was less sensitive at higher values of *Pr*. Dhiman *et al.* (2006) analyzed the forced convective steady flow past a square cylinder to elucidate the influence of *Pr* on heat transfer characteristics for 0.7 < *Pr* < 4000. They presented a heat transfer correlation for constant temperature and constant heat flux cases.

It can be concluded from the above discussion that limited studies have been performed to understand the influence of *Pr* on flow past a square cylinder. To the best of our knowledge, no study has been performed to examine the influence of *Pr* on a cross buoyancy flow past a heated square cylinder placed in a free-stream in unsteady, laminar flow regime. The present study attempts to fill this gap. In the present study flow past a heated square cylinder is studied for 0.02 < *Pr* < 100 at *Re* = 100 and *Ri* = 1. The problem statement and formulation are presented in Section 2. Computational methodology is discussed in Section 3. Results and discussion are presented in Section 4 and conclusions are provided in Section 5.

2. PROBLEM STATEMENT AND FORMULATION

A two-dimensional stationary square cylinder of side D is placed in a free-stream at distances of $L_u = 7.5D$ and $L_d = 35D$ from the inlet and outlet boundaries, respectively (Fig. 1). For making the flow configuration computationally feasible two artificial slip boundaries (top and bottom) were placed above and below the cylinder, both at a distance of $L_h/2$ from the cylinder center. Previous studies (Sohankar *et al.* 1998; Chatterjee and Mondal 2012) have established that the effect of artificial boundaries are negligible on the flow around a cylinder for $L_h = 20D$. The cylinder was kept at a constant temperature of T_h while the free-stream temperature was T_∞ ($T_h > T_\infty$). The free-stream velocity U_∞ was in the positive x-direction while the buoyancy acted in the negative y-direction (downward). Since difference between the cylinder and free-stream temperatures was small, density was assumed to be constant everywhere except in the body force term (the Boussinesq approximation).

For two-dimensional, incompressible, laminar flow the non-dimensional governing equations may be written as

1. Continuity:

$$\frac{\partial u}{\partial x} + \frac{\partial v}{\partial y} = 0 \tag{1}$$

2. Momentum:

$$\frac{\partial u}{\partial t} + \frac{\partial (uu)}{\partial x} + \frac{\partial (uv)}{\partial y} = -\frac{\partial p}{\partial x} + \frac{1}{Re}\left(\frac{\partial^2 u}{\partial x^2} + \frac{\partial^2 u}{\partial y^2}\right) \tag{2}$$

$$\frac{\partial v}{\partial t} + \frac{\partial (uv)}{\partial x} + \frac{\partial (vv)}{\partial y} = -\frac{\partial p}{\partial x} + \frac{1}{Re}\left(\frac{\partial^2 v}{\partial x^2} + \frac{\partial^2 v}{\partial y^2}\right) + Ri\theta \tag{3}$$

3. Energy:

$$\frac{\partial\theta}{\partial t}+\frac{\partial(u\theta)}{\partial x}+\frac{\partial(v\theta)}{\partial y}=\frac{1}{RePr}\left(\frac{\partial^2\theta}{\partial x^2}+\frac{\partial^2\theta}{\partial y^2}\right) \quad (4)$$

In case of a 2D flow, the vorticity has only one component perpendicular to the plane of flow. In a 2D flow, the vorticity transport equation may be written as

$$\frac{\partial\omega}{\partial t}+u\frac{\partial\omega}{\partial x}+v\frac{\partial\omega}{\partial y}=Ri\frac{\partial\theta}{\partial x}+\frac{1}{Re}\left(\frac{\partial^2\omega}{\partial x^2}+\frac{\partial^2\omega}{\partial y^2}\right) \quad (5)$$

where, $Ri\frac{\partial\theta}{\partial x}$ denotes the production of vorticity due to buoyancy, also called the baroclinic production.

The non-dimensional variables are defined as:

$$x=\frac{\bar{x}}{D},\quad y=\frac{\bar{y}}{D},\quad u=\frac{\bar{u}}{U_\infty},v=\frac{\bar{v}}{U_\infty}$$

$$p=\frac{\bar{p}}{\rho{U_\infty}^2},\qquad \theta=\frac{T-T_\infty}{T_h-T_\infty},\qquad t=\frac{U_\infty\bar{t}}{D}$$

where the quantities with the overbar denote dimensional variables.

Boundary conditions:

- Inlet: uniform flow, $u = 1$, $v = 0$ and $\Theta = 0$.
- Outlet: advective, $\frac{\partial\phi}{\partial t}+U\frac{\partial\phi}{\partial x}=0$, where Φ is u, v or Θ.
- Cylinder: no slip, $u = 0$, $v = 0$ and $\Theta = 1$.
- Top: slip, $\frac{\partial u}{\partial y}=v=0$ and $\frac{\partial\theta}{\partial y}=0$.
- Bottom: slip, $\frac{\partial u}{\partial y}=v=0$ and $\frac{\partial\theta}{\partial y}=0$.

3. COMPUTATIONAL METHODOLOGY

The finite volume based open source code OpenFOAM was used for simulations. The unsteady terms were discretized implicitly by using the second-order backward scheme. For the convective terms the third order accurate QUICK scheme was used in both momentum and energy equations. The central difference scheme was used to discretize the diffusion terms. In order to obtain values at face centers from cell centers, linear interpolation was used (OpenFOAM Programmer's Guide 2009). An advanced PIMPLE algorithm (OpenFOAM User Guide 2009), which is a combination of SIMPLE and PISO, was used to handle the pressure-velocity coupling. The resultant algebraic equations were solved by using a geometric algebraic multigrid solver while the Gauss-Seidel method was used as a smoother.

A non-uniform orthogonal grid was used for computations. A very fine grid was used near the cylinder surfaces to accurately capture the flow field. Since the thickness of the thermal boundary-layer was quite small at high values of *Pr*, for accurately capturing the flow characteristics grids of size approximately equal to 0.005*D* were used in the vicinity of cylinder. However, in the far field slightly coarser grids were used. The computational domain with the grid distribution is shown in Fig. 2. The time step (Δt) was selected in such a way that the Courant number ($\frac{u\Delta t}{\Delta x}$) was less than 1 in the entire computational domain.

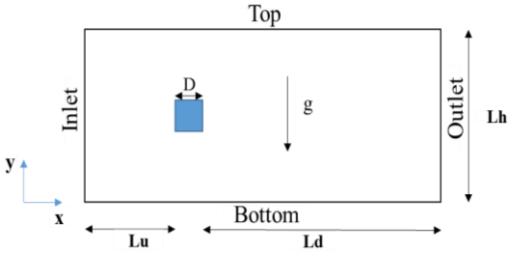

Fig. 1. Computational domain for cross buoyancy flow past a square cylinder.

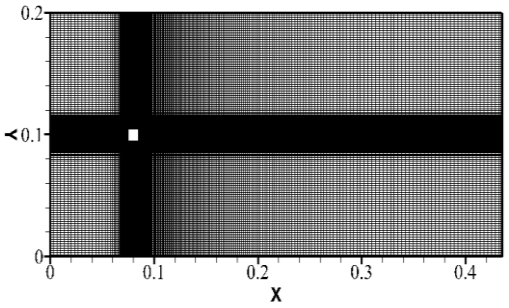

Fig. 2. Non-uniform computational grid structure.

The grid independence study was carried out to choose an optimal grid size. Four grids with 280x200, 330x250, 380x300 and 664x496 cells in the *x* and *y* directions, respectively, were assessed. The mean drag coefficient (C_D) and Strouhal number (*St*) obtained for flow past a square cylinder at *Re* = 100, *Ri* = 1 and *Pr* = 1 using these grids are presented in Table 1. On the basis of the obtained results a grid of size 330x250 was used for the subsequent simulations.

Table 1 Values of C_D and *St* for different meshes

S. No.	Grid size	Drag coefficient (C_D)	Strouhal number (*St*)
1	280x200	1.71	0.130
2	330x250	1.72	0.134
3	380x300	1.72	0.134
4	664x496	1.72	0.134

4. RESULTS AND DISCUSSION

The code used for the present computations was validated with the reported experimental and numerical results (Robichaux *et al* 1999; Sharma and Eswaran 2004a; Bhattacharyya and Mahapatra 2005). Figs. 3 and 4 show variation of the mean drag coefficient and mean Nusselt number, respectively, on the cylinder surfaces with *Re* for flow past a square cylinder placed in a free-stream.

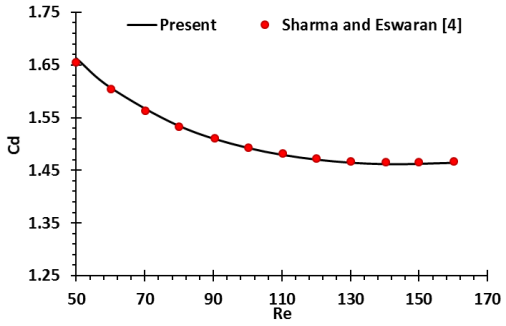

Fig. 3. Variation of mean drag coefficient with *Re*.

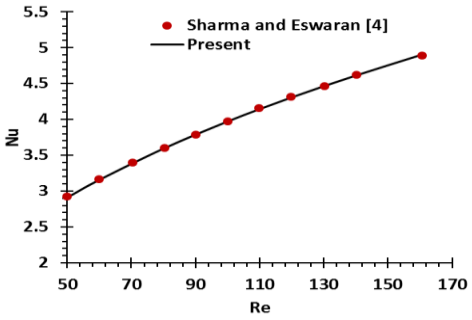

Fig. 4. Variation of mean Nusselt number on the cylinder surface with *Re*.

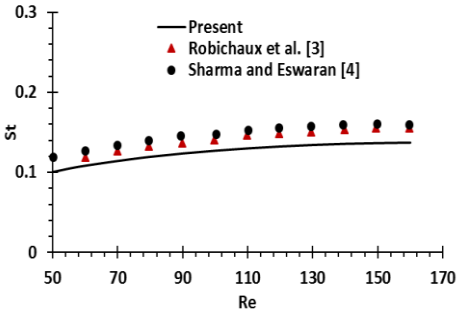

Fig. 5. Variation of mean Strouhal number with *Re*.

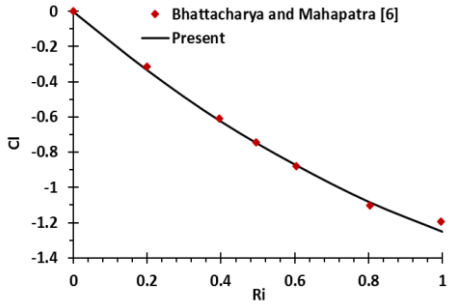

Fig. 6. Variation of mean lift coefficient with *Ri* at *Re* = 100.

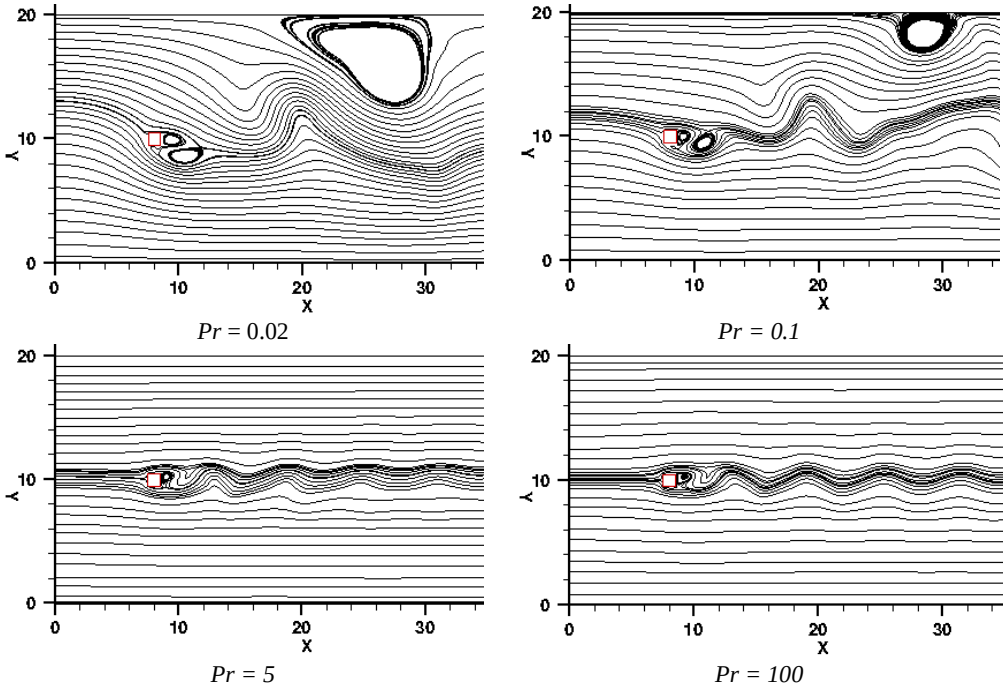

Fig. 7. Instantaneous streamlines for various values of *Pr* at *Ri* = 1 and *Re* = 100.

Figure 5 presents a variation of Strouhal number with *Re*. It can be observed from Figs. 3-5 that the results obtained by the present code are in good agreement with the reported studies. The present code has been further tested for a mixed convection flow. Figure 6 presents a variation of the mean lift coefficient with *Ri* for flow past a square cylinder placed in a free-stream at *Re* = 100. The lift coefficient is in good agreement with the results of Bhattacharya and Mahapatra (2005).

4.1 Flow Pattern

Figure 7 presents the instantaneous streamlines for the flow past a heated square cylinder at various values of *Pr*. Unsteadiness in the entire domain for low values of *Pr* can be observed in Fig. 7. As the

value of *Pr* is increased, the unsteadiness is confined near the centerline of the domain. Since at low values of *Pr*, the diffusive term in the energy equation is dominant and influence of buoyancy is large, it results in unsteadiness in the entire domain. At higher values of *Pr*, the convective term is more dominant in the energy equation which diminishes the influence of buoyancy in the far field and hence, unsteadiness is confined to the vicinity of the domain centerline. In the present study the top and bottom boundaries were considered as the slip surfaces. These were mathematically represented as $\frac{\partial u}{\partial y} = v = 0$, which means a frictionless wall. Due to the presence of a frictionless wall (slip) recirculation zones appear near the top boundary of the domain at low values of *Pr* and similar behavior was also reported in the case of a circular cylinder by Biswas and Sarkar (2009). These recirculation zones are formed due to a strong action of buoyancy which causes a positive vortex formation near the cylinder to advect upward. These recirculation zones advect with the vortex (Fig. 8). At *Pr* = 0.02 the effect of buoyancy is so large that the recirculation zone breaks into two parts (Fig. 9) while at *Pr* = 0.1 the recirculation zone is simply advected downstream.

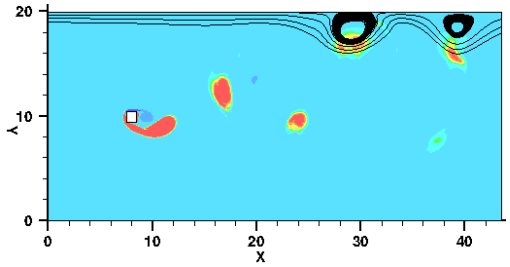

Fig. 8. Instantaneous streamlines and contours of vorticity at *Pr* = 0.1.

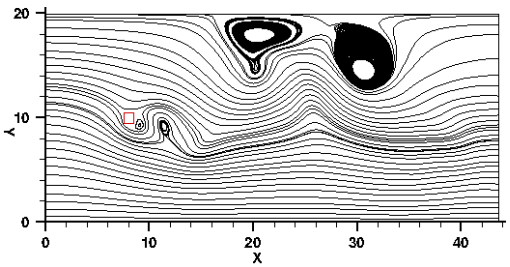

Fig. 9. Instantaneous streamlines at *Pr* = 0.02.

Figure 10 presents time-averaged streamlines for the flow over a heated square cylinder at different values of *Pr* at a fixed *Ri* = 1. It can be observed from Fig. 10 that at low values of *Pr* the flow fields are quite influenced by buoyancy and are asymmetric. The incoming streamlines get deflected downward and hence more amount of fluid passes from the lower region of the cylinder than that from the upper region. Therefore, velocity near the bottom face of the cylinder is higher than that near the top face of the cylinder (Fig. 11). However, at high values of *Pr*, the downward deflection of incoming streamlines decreases and at very high values of *Pr* the flow becomes nearly symmetric. At lower values of *Pr* a large recirculation zone is formed near the bottom face of the cylinder and this recirculation zone disappears at high values of *Pr*.

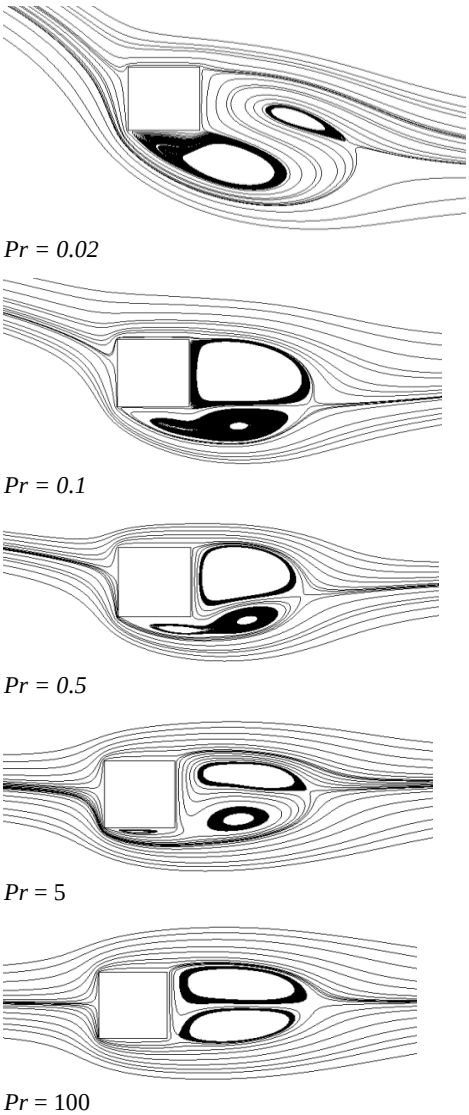

Fig. 10. Time-averaged streamlines for various values of *Pr* at *Ri* = 1 and *Re* = 100.

4.2 Temperature Field

Figure 12 shows instantaneous contours of temperature field at various values of *Pr*. The temperature contours are similar to vorticity contours (Fig. 13). However, for *Pr* < 1 the vorticity contours are more compact than temperature contours, since for *Pr* < 1 the thermal diffusivity is larger than the momentum diffusivity (Fig. 13). At high values of *Pr* the thermal blobs that originate from the cylinder surface get advected downstream in a compact form since at high values of *Pr* the diffusion term in the energy equation is relatively small. Temperature contours originate from the cylinder surface in the form of hot blobs. These hot

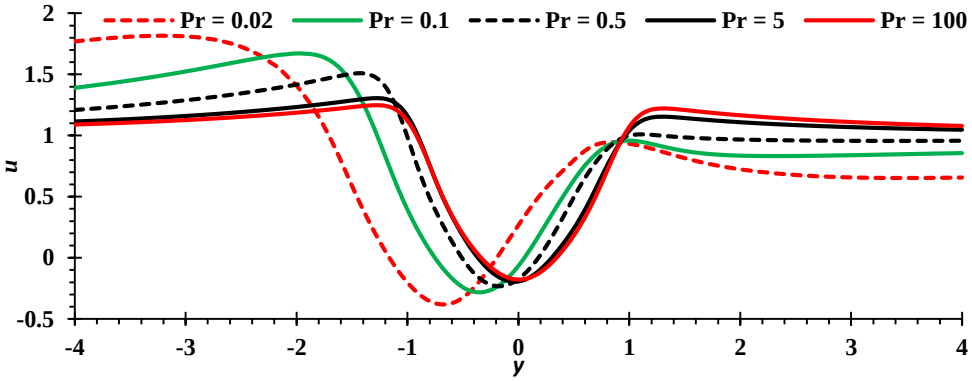

Fig. 11. Time-averaged streamwise velocity at distance of *1 D* from rear face of the cylinder.

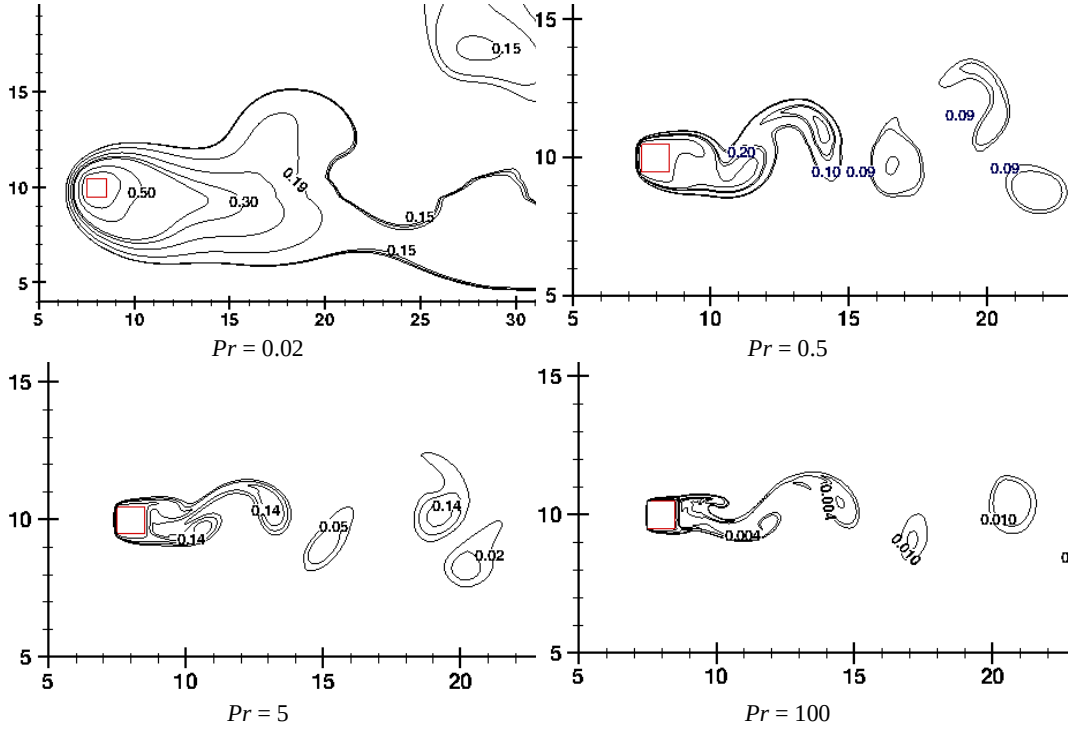

Fig. 12. Instantaneous temperature contours at various values of *Pr* at *Ri* = 1.

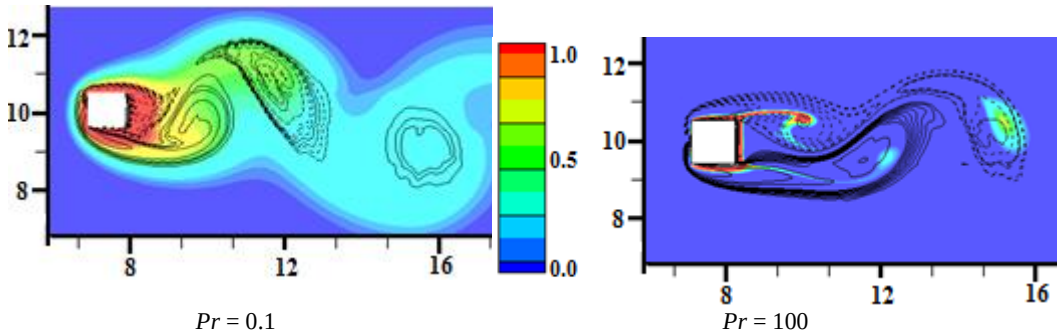

Fig. 13. Instantaneous temperature (flooded) and vorticity (lines) contours.

blobs are trapped in the detached vortices and are advected downstream with vortices. At low values of *Pr*, due to a dominant effect of buoyancy, these hot blobs move upward. Since influence of buoyancy diminishes at higher values of *Pr*, the upward motion of hot blobs decreases with an increase in the value

of *Pr*. At *Pr* = 0.02, a hot blob is advected with the vortex near the top boundary of the domain due to a strong upward motion and this behaviour is discussed in Section 4.2. At *Pr* = 100, temperature contours originate from the boundary-layer in the form of streaks, since at high values of *Pr* the advection term is more dominant than the diffusion term in the boundary-layer.

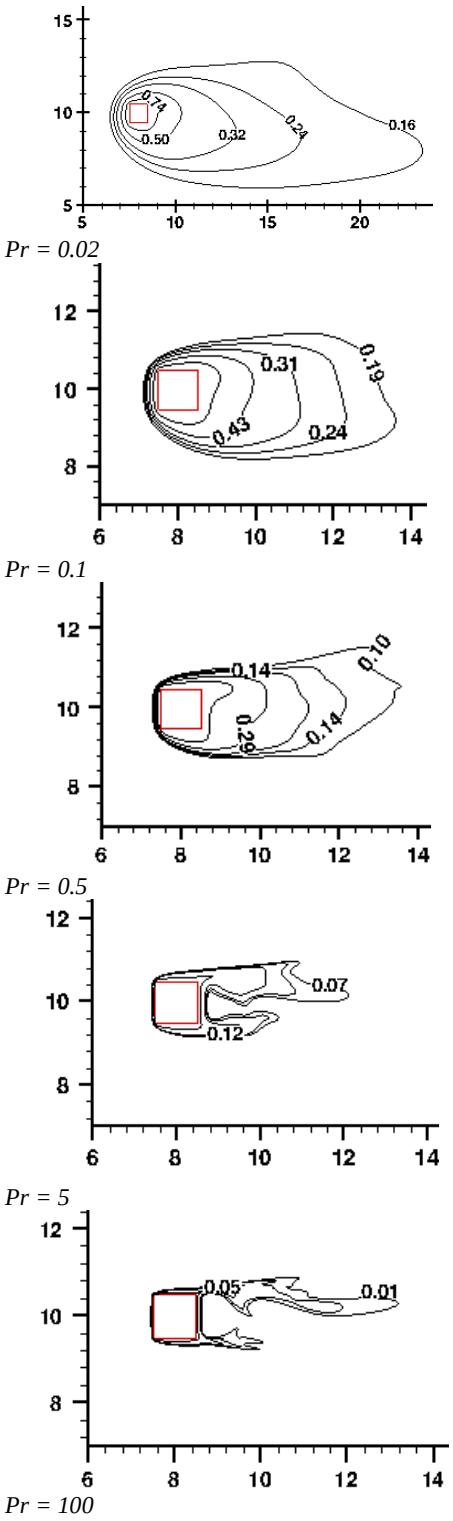

Fig. 14 Time-averaged temperature contours at various values of *Pr* at *Ri* = 1.

Figure 13 shows that the temperature of the upper blob is larger than that of the lower blob. The difference in temperature can be explained by using the time-averaged streamlines. As shown in Fig. 10 some upward directed streamlines are present in the upper blob region. These streamlines enhance heat transfer from the cylinder into the upper blob. In the region of lower blob, no such streamlines are present and therefore heat transfer from the cylinder into the lower blob area is not much effective. At lower value of *Pr* the diffusion term is more effective and more heat is transferred from the cylinder into these blobs. Therefore, blobs are more heated at lower values of *Pr* compared to higher values of *Pr*.

Figure 14 shows the time-averaged temperature contours for various values of *Pr*. At lower values of *Pr*, the thickness of thermal-boundary layer on the cylinder is large, which increases the transverse width of the contours. At the front face of the cylinder contours are crowded, which shows that the thermal boundary-layer is thin and heat transfer is maximum from this surface. At the rear face of the cylinder the shapes of the contours are convex for lower values of *Pr* and concave for larger values of *Pr*. This behavior indicates that the interaction between the vortex is large at lower values of *Pr* and it decreases at higher values of *Pr*.

4.3 Formation of Vortex

Vortex structure emerges from the boundary-layer formed at the cylinder surfaces in the form of a strand with a coherent blob at the strand tip. These strands are advected from the boundary-layer into the wake region. In the wake, constriction of the strand occurs due to the presence of large strain rate. Constriction process causes the strand to be separated from the boundary-layer and advected downstream in the form of a coherent blob (Gerrard 1966). The constriction process is described by a variable ζ defined as

$$\zeta = {}^{1}/_{2}\left(\left(\frac{\partial u}{\partial x}-\frac{\partial v}{\partial y}\right)^2+\left(\frac{\partial v}{\partial x}+\frac{\partial u}{\partial y}\right)^2-\left(\frac{\partial v}{\partial x}-\frac{\partial u}{\partial y}\right)^2\right) \tag{6}$$

The constriction process takes place in the region where $\zeta > 0$ which shows area of high strain rate and the accumulation of vortex occurs where $\zeta < 0$ (Kieft *et al.* 2007). Figure 15 shows distribution of vorticity and ζ for two different values of *Pr* for the same value of *Ri*. At $t = 0$ constriction of upper vortex takes place (Fig. 15). The constriction area coincides with a positive value of ζ while negative value of ζ occurs at the vortex tip. Similarly, at $t = T/2$ constriction of lower vortex takes place. At high values of *Pr* the constriction and accumulation processes take place at a larger distance from the cylinder than that at low values of *Pr* (Fig. 15). Hence vortex extreme occurs more downstream for higher value of *Pr* than that for lower values of *Pr*.

4.4 Baroclinic Production

There are two sources of vorticity production in a mixed convection flow: due to wall shear and due to buoyancy (baroclinic production). Figure 16 shows

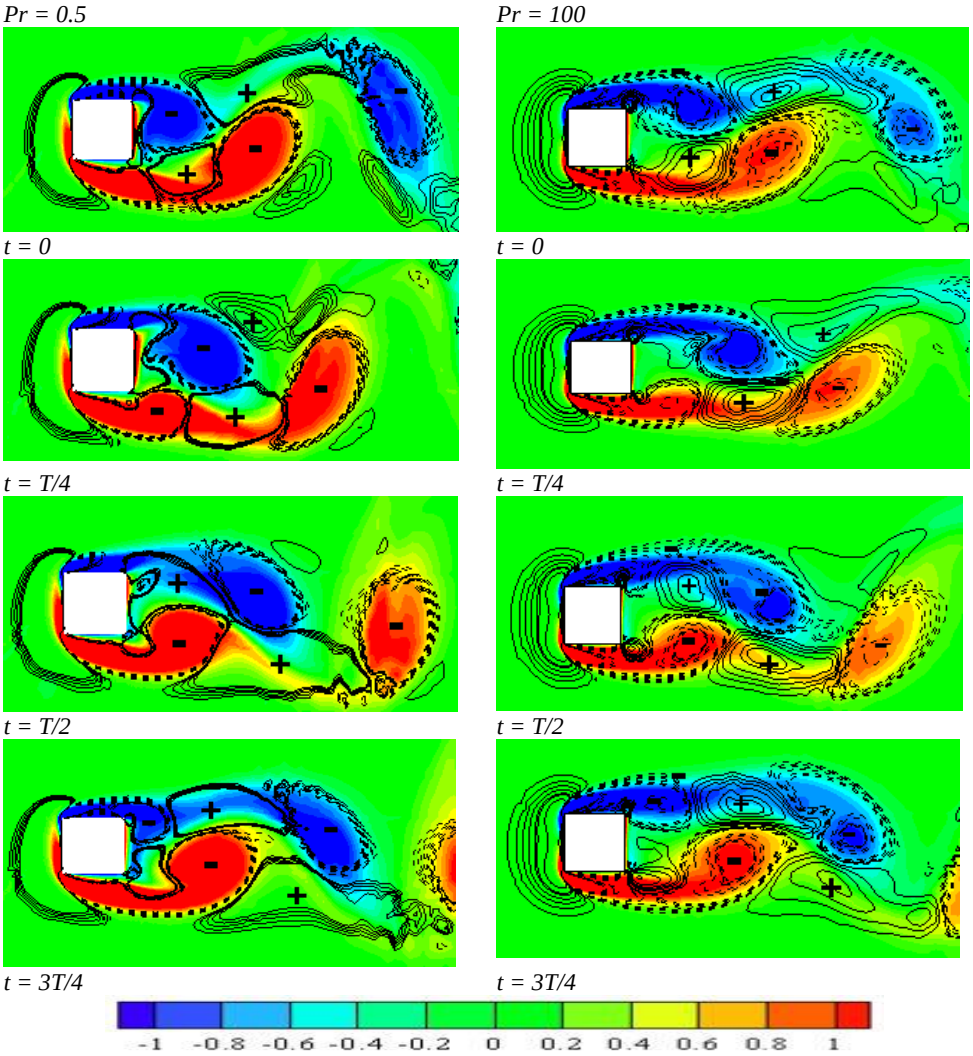

Fig. 15. Instantaneous contours of vorticity (flooded) and ζ(lines).

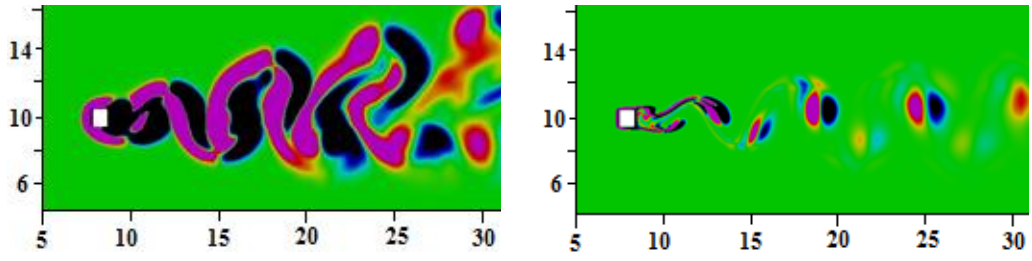

Pr = 0.5 *Pr* = 100

Fig. 16. Baroclinic production of vorticity at two different values of *Pr*.

instantaneous contours of the vorticity production due to buoyancy, termed as the baroclinic production (Kieft *et al.* 2007), at two different values of *Pr*. At low values of *Pr* the transverse width of the vorticity production increases downstream. While at high values of *Pr*, the vorticity is produced close to the centerline of the domain only. This behavior is because at low values of *Pr*, hot blobs are advected upwards due to a strong action of buoyancy, which causes a temperature gradient in the streamwise direction and it is responsible for the baroclinic production in the region away from the centerline. At high values of *Pr*, hot blobs cannot advect away from the centerline since influence of buoyancy is weak. Hence, streamwise temperature gradient does not exist in the region away from the centerline and no baroclinic production occurs. Further, the regions of positive and negative baroclinic productions occur alternately. This behavior is because temperature is advected in the form of hot blobs and this causes positive and negative temperature gradients upstream and downstream of the blobs, respectively. Hence baroclinic production is positive upstream and negative downstream of blobs.

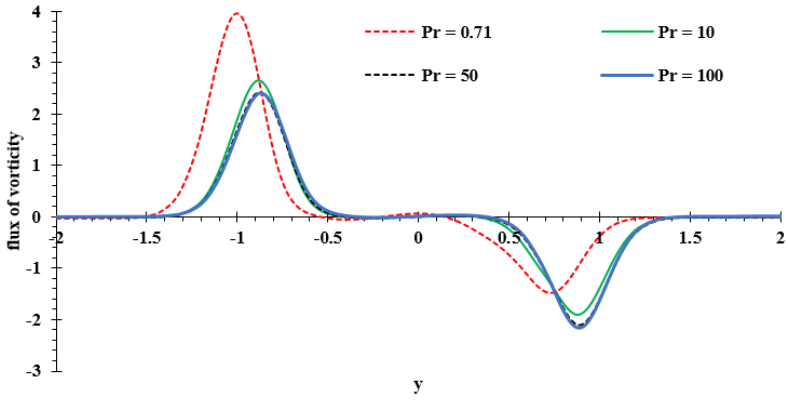

Fig. 17. Time-averaged flux of vorticity at the vertical cross-section x = 1.

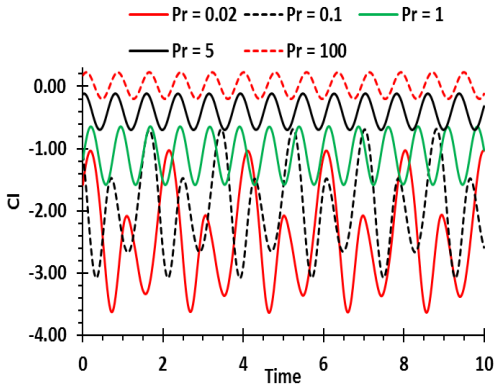

Fig. 18. Variation of instantaneous lift coefficient.

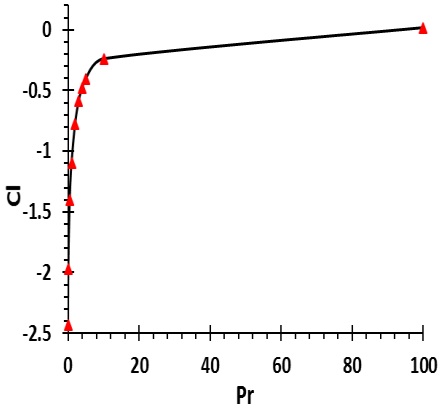

Fig. 19. Variation of mean lift coefficient with *Pr*.

For investigating the cumulative outcome of the baroclinic vorticity near the cylinder surfaces and advection of the wall vorticity, the time-averaged flux of vorticity through a transverse cross-section at a fixed value of x is calculated (Kieft *et al.* 2003). It represents the amount of vorticity captured in the vortices which were generated upstream of a given cross-section. Figure 17 represents the time-averaged flux of vorticity at x = 1 for various values of *Pr*. It can be observed that the flux of vorticity is positive in the lower half of wake and the value of this flux increases with a decrease in *Pr* and the location of the maximum flux is shifted downward (Fig. 17). In the upper half of wake the flux of vorticity is negative and the maximum magnitude of this flux increases with *Pr*. Further, the location of the maximum negative flux is shifted upwards.

4.5 Force Coefficients

There are two main factors due to which a cylinder experiences a lift force. Firstly, the vortex shedding from the top and bottom faces of the cylinder. In case of a mixed convection, the strength of the upper vortex is larger than that of the lower vortex. Hence, cylinder experiences a net positive lift due to vortex shedding. Secondly, the incoming streamlines get deflected downward due to buoyancy causing large amount of fluid to pass from the bottom region of the cylinder. Due to this behaviour, the velocity near the bottom face of the cylinder rises and pressure decreases. This decrease in pressure causes a net pressure difference between the top and bottom faces of the cylinder and hence, a net negative lift is generated. As discussed in Section 4.1, the incoming streamlines get deflected downward at lower values of *Pr*. The negative lift generated due to this deflection is more dominant compared to the positive lift generated due to an asymmetric vortex shedding. Consequently, at small values of *Pr* the cylinder experiences a net negative lift (Figs. 18 - 19). Since, with an increase in the value of *Pr*, the downward deflection of the incoming streamlines decreases and hence lift generated by this deflection is comparable to the lift generated by asymmetric vortex shedding. Hence, at higher values of *Pr* the magnitude of the downward lift decreases (Fig. 19). Further, at lower values of *Pr*, the lift force changes rapidly with an increase in the value of *Pr*. At *Pr* = 1000, the streamlines are almost symmetric and the lift generated by asymmetric vortex shedding is dominant than the lift generated by the deflection of streamlines. Hence, the net lift force is positive for very high values of *Pr* (Fig. 19).

Figure 20 shows variation of the drag coefficient (C_D) with time. Since at lower values of *Pr* the strength of the vortex at the bottom surface is weak, only one peak is present in C_D. As the value of *Pr* is

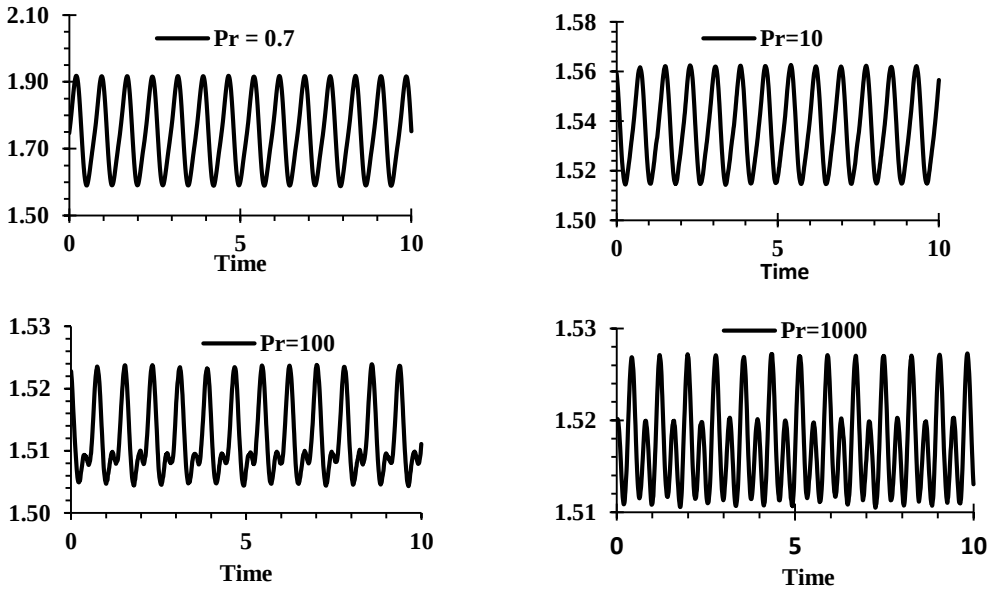

Fig. 20. Variation of instantaneous drag coefficient with *Pr*.

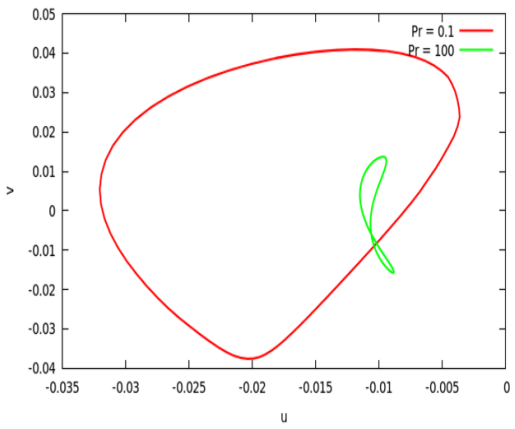

Fig. 22. Phase diagram for *Pr* = 0.1 and *Pr* = 100 at *Ri* = 1 and *Re* = 100.

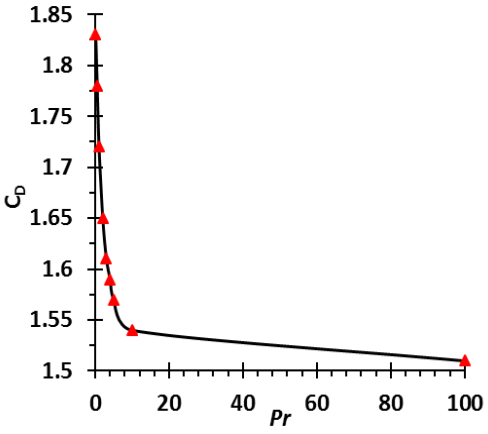

Fig. 21. Variation of mean drag coefficient with *Pr*.

increased the strength of lower vortex becomes strong and hence two peaks are present in C_D (Fig. 20). Figure 21 shows a variation of mean C_D with *Pr*. Net C_D decreases rapidly with an increase in *Pr* at lower values of *Pr*.

4.6 Phase Portraits

Figure 22 shows the velocity phase portraits for two different values of *Pr* at the same value of *Ri*. These phase portraits were drawn by measuring the streamwise and transverse velocities at a distance of 0.5*D* from the rear surface of the cylinder. The phase portraits are closed curves showing that the flow is periodic. It can be observed from Fig. 22 that at low values of *Pr* both streamwise and transverse velocities fluctuate with large amplitude and at high values of *Pr* amplitudes reduce to small values. Another important information that can be deduced from the phase portrait is that the area under the phase portrait represents the energy transport due to heat (Chatterjee and Mondal 2011). Since the area under the phase portraits is larger at small values of *Pr* than that at large values of *Pr*, the energy transfer due to heat is large at low values of *Pr*.

4.7 Strouhal Number

Figure 23 shows variation of Strouhal number with *Pr*. At low values of *Pr*, Strouhal number first increases with *Pr* then decreases and it becomes constant at high values of *Pr* which is also reported in the case of a circular cylinder (Sarkar *et al.* 2011). It shows that the momentum transfer from the boundary-layer to the vortex is quite sensitive at low values of *Pr*. It first decreases and then increases

with an increase in the value of *Pr*.

4.8 Nusselt Number

Figure 24 shows the time-averaged Nusselt number on the cylinder. As expected, *Nu* increases with *Pr*, since the thickness of thermal boundary-layer decreases and temperature gradient on the cylinder surfaces increases with an increment in *Pr*. Figure 25 shows the time-averaged Nusselt number on surfaces of the cylinder. On each surfaces *Nu* increases with *Pr*. The value of *Nu* is maximum at the front surface which can also be concluded by looking at the temperature contours which are quite dense near the front surface. The value of *Nu* is minimum on the bottom surface due to the formation of a recirculation zone near the surface. This recirculation zone hinders the cooled fluid to come in contact with the bottom surface and hence reduces heat transfer from the surface.

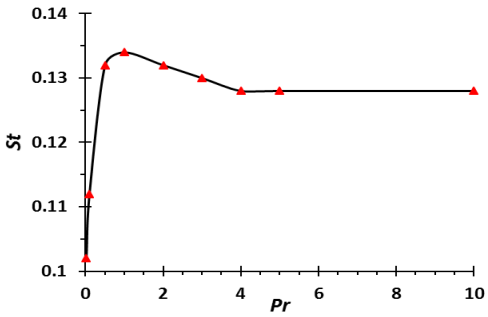

Fig. 23. Variation of Strouhal number with *Pr*.

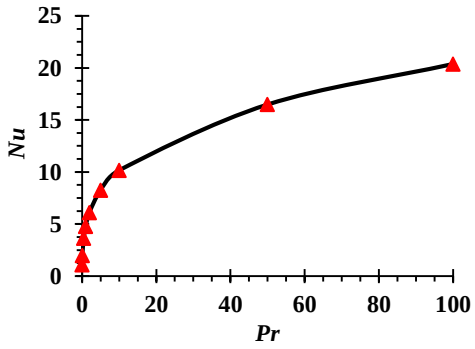

Fig. 24. Variation of time-averaged Nusselt number on the cylinder with *Pr*.

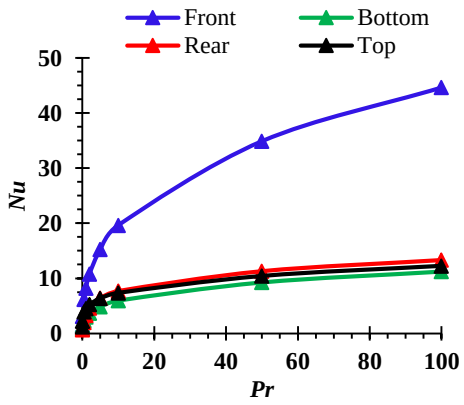

Fig. 25. Nusselt number on each surfaces of the cylinder.

5. CONCLUSIONS

Influence of Prandtl number *(Pr)* on a cross buoyancy flow past a heated square cylinder has been studied in the present paper. At low values of *Pr* the influence of buoyancy was large which caused asymmetry in the flow field with incoming streamlines deflected downwards. At high values of *Pr*, the flow field was stabilized and returned towards symmetry due to a weak influence of buoyancy. Isotherms and vorticity contours were similar but isotherms were more diffusive at low values of *Pr* and these were compact at higher values of *Pr*. Vortex were quite heated at low values of *Pr* due to large diffusion of heat from the cylinder. The baroclinic production was strongly altered with values of *Pr*. The transverse extent of the baroclinic production increased downstream at low values of *Pr* while it was confined close to the domain centerline at high values of *Pr*. The lift coefficient was found to be negative at low values of *Pr* and it became less negative with an increase in the value of *Pr*. Further, at very high values of *Pr* the net lift became slightly positive. This behavior could be possibly due to a difference in the vortex strength. Mean drag coefficient decreased with an increase in *Pr* and became a constant at very high values of *Pr*. Strouhal number was quite sensitive at low values of *Pr*.

ACKNOWLEDGMENT

The first author would like to thank Council of Scientific & Industrial Research, New Delhi, India for providing financial support through the award of Junior Research Fellowship [Ref. 09/086(1244)/2015-EMR-I].

REFERENCES

Bhattacharyya, S. and S. Mahapatra (2005). Vortex shedding around a heated square cylinder under the influence of buoyancy. *Heat and Mass Transfer* 41, 824-833.

Biswas, G. and S. Sarkar (2009). Effect of thermal buoyancy on vortex shedding past a circular cylinder in cross-flow at low Reynolds numbers. *International Journal of Heat and Mass Transfer* 52, 1897-1912.

Chatterjee, D. (2014). Dual role of thermal buoyancy in controlling boundary layer separation around bluff obstacles. *International Communications in Heat and Mass Transfer* 56, 152-158.

Chatterjee, D. and B. Mondal (2011). Effect of thermal buoyancy on vortex shedding behind a square cylinder in cross flow at low Reynolds numbers. *International Journal of Heat and Mass Transfer* 54, 5262-5274.

Chatterjee, D. and B. Mondal (2012). Effect of thermal buoyancy on the two-dimensional upward flow and heat transfer around a square cylinder. *Heat Transfer Engineering* 33, 1063-1074.

Chatterjee, D. and G. Biswas (2011). The effects of Reynolds and Prandtl numbers on flow and heat transfer across tandem square cylinders in the steady flow regime. *Numerical Heat Transfer, Part A: Applications* 59, 421-437.

Chatterjee, D. and S. Amiroudine (2010). Two-dimensional mixed convection heat transfer from confined tandem square cylinders in cross-flow at low Reynolds numbers. *International Communications in Heat and Mass Transfer* 37, 7-16.

Cheng, M., D. S. Whyte and J. Lou (2007). Numerical simulation of flow around a square cylinder in uniform-shear flow. *Journal of Fluids and Structures* 23, 207-226.

Dhiman, A. K., R. P. Chhabra, A. Sharma and V. Eswaran (2006). Effects of Reynolds and Prandtl numbers on heat transfer across a square cylinder in the steady flow regime. *Numerical Heat Transfer, Part A: Applications* 49, 717-731.

Dhiman, A. K., R. P. Chhabra and V. Eswaran (2008). Steady mixed convection across a confined square cylinder. *International Communications in Heat and Mass Transfer* 35, 47-55.

Franke, R., W. Rodi and B. Schönung (1990). Numerical calculation of laminar vortex-shedding flow past cylinders. *Journal of Wind Engineering and Industrial Aerodynamics* 35, 237-257.

Gerrard, J. H. (1966). The mechanics of the formation region of vortices behind bluff bodies. *Journal of Fluid Mechanics* 25, 401-413.

Hassan, N. and R. Ali (2013). Vortex-shedding suppression in two-dimensional mixed convective flows past circular and square cylinders. *Physics of Fluids* 25, 88.

Igarashi, T. (1987). Fluid flow and heat transfer around rectangular cylinders (the case of a width/height ratio of a section of 0.33~1.5). *International Journal of Heat and Mass Transfer* 30, 893-901.

Kakade, A. A., S. K. Singh, P. K. Panigrahi and K. Muralidhar (2010). Schlieren investigation of the square cylinder wake: Joint influence of buoyancy and orientation. *Physics of Fluids* 22, 054-107.

Kieft, R. N., C. C. M. Rindt and A. A. Van Steenhoven (2007). Near-wake effects of a heat input on the vortex-shedding mechanism. *International Journal of Heat and Fluid Flow* 28, 938-947.

Kieft, R. N., C. C. M. Rindt, A. A. Van Steenhoven and G. J. F. Van Heijst (2003). On the wake structure behind a heated horizontal cylinder in cross-flow. *Journal of Fluid Mechanics* 486, 189-211.

Lyn, D. A. and W. Rodi (1994). The flapping shear layer formed by flow separation from the forward corner of a square cylinder. *Journal of Fluid Mechanics* 267, 353-376.

Nakaguchi, H., K. Hashimoto and S. Muto (1968). An experimental study on aerodynamic drag of rectangular cylinders. *The Journal of the Japan Society of Aeronautical Engineering* 16, 1-5.

Norberg, C., A. Sohankar and L. Davidson (1995). Numerical simulation of unsteady flows around a square two-dimensional cylinder. In *Twelfth Australian Fluid Mechanics Conference*, 517-520.

OpenCFD L.t.d. (2011). OpenFOAM - The Open Source CFD Toolbox, Version 3.0.

OpenCFD L.t.d. (2011). OpenFOAM - The Open Source CFD Toolbox, Version 3.0.

Rahnama, M. and H. Hadi Moghaddam (2005). Numerical investigation of convective heat transfer in unsteady laminar flow over a square cylinder in a channel. *Heat Transfer Engineering* 26, 21-29.

Ranjan, P. and A. Dewan (2016). Effect of side ratio on fluid flow and heat transfer from rectangular cylinders using the PANS method. *International Journal of Heat and Fluid Flow* 61, 309-322.

Robichaux, J., S. Balachandar and S. P. Vanka (1999). Three-dimensional Floquet instability of the wake of square cylinder. *Physics of Fluids* 11, 560-578.

Sahu, A. K., R. P. Chhabra and V. Eswaran (2009). Effects of Reynolds and Prandtl numbers on heat transfer from a square cylinder in the unsteady flow regime. *International Journal of Heat and Mass Transfer* 52, 839-850.

Sarkar, S., A. Dalal and G. Biswas (2011). Unsteady wake dynamics and heat transfer in forced and mixed convection past a circular cylinder in cross flow for high Prandtl numbers. *International Journal of Heat and Mass Transfer* 54, 3536-3551.

Sharma, A. and V. Eswaran (2004a) Heat and fluid flow across a square cylinder in the two-dimensional laminar flow regime. *Numerical Heat Transfer, Part A: Applications* 45, 247-269.

Sharma, A. and V. Eswaran (2004b). Effect of aiding and opposing buoyancy on the heat and fluid flow across a square cylinder at Re = 100. *Numerical Heat Transfer, Part A: Applications* 45, 601-624.

Sharma, N., A. K. Dhiman and S. Kumar (2012). Mixed convection flow and heat transfer across a square cylinder under the influence of aiding buoyancy at low Reynolds numbers. *International Journal of Heat and Mass Transfer* 55, 2601-2614.

Singh, S. K., P. K. Panigrahi and K. Muralidhar (2007). Effect of buoyancy on the wakes of circular and square cylinders: a schlieren-

interferometric study. *Experiments in Fluids* 43, 101-123.

Sohankar, A., C. Norberg and L. Davidson (1998). Low-Reynolds-number flow around a square cylinder at incidence: study of blockage, onset of vortex shedding and outlet boundary condition. *International Journal for Numerical Methods in Fluids* 26, 39-56.